Photoabsorption of the molecular IH cation at the iodine 3*d* absorption edge

Stephan Klumpp,[1,2,*] Alexander A. Guda,[3] Kaja Schubert,[4,2] Karolin Mertens,[2] Jonas Hellhund,[5] Alfred Müller,[5] Stefan Schippers,[6] Sadia Bari,[4] and Michael Martins[2,†]

[1]*FS-FLASH-D, Deutsches Elektronen-Synchrotron (DESY), Notkestrasse 85, 22607 Hamburg, Germany*

[2]*Department Physik, Universität Hamburg, Luruper Chaussee 149, 22761 Hamburg, Germany*

[3]*International Research Center "Smart Materials", Southern Federal University, ul. Andreya Sladkova 178/24, 344090 Rostov-on-Don, Russia*

[4]*FS-SCS, Deutsches Elektronen-Synchrotron (DESY), Notkestrasse 85, 22607 Hamburg, Germany*

[5]*Institut für Atom- und Molekülphysik, Justus-Liebig-Universität Gießen, Leihgesterner Weg 217, 35392 Giessen, Germany*

[6]*I. Physikalisches Institut, Heinrich-Buff-Ring 16, Justus-Liebig-Universität Gießen, 35392 Giessen, Germany*

(Received 3 March 2017; revised manuscript received 6 December 2017; published 1 March 2018)

Yields of atomic iodine I^{q+} ($q \geqslant 2$) fragments resulting from photoexcitation and photoionization of the target ions IH^+ and I^+ have been measured in the photon-energy range 610–680 eV, which comprises the thresholds for iodine 3*d* ionization. The measured ion-yield spectra show two strong and broad resonance features due to the excitation of the $3d_{3/2,5/2}$ electrons into εf states rather similar for both parent ions. In the 3*d* pre-edge range, excitations into $(np\,\pi)$-like orbitals and into an additional σ^* orbital are found for IH^+, which have been identified by comparison of the atomic I^+ and molecular IH^+ data and with the help of (time-dependent) density functional theory (DFT) and atomic Hartree-Fock calculations. The $(5p\,\pi)$ orbital is almost atomlike, whereas all other resonances of the IH^+ primary ion show a more pronounced molecular character, which is deduced from the chemical shifts of the resonances and the theoretical analysis.

DOI: 10.1103/PhysRevA.97.033401

I. INTRODUCTION

Molecular ions are of high interest due to the role they generally play in chemistry, e.g., in batteries [1] or enzymatic reactions [2]. Molecular ions can also occur as transients in dynamic molecular processes, as investigated by transient inner-shell photoabsorption spectroscopy (e.g., [3]). Moreover, molecular ions have been identified in space, where they are important for the chemistry in many cosmic environments [4] and where they are created by the impact of cosmic rays or by ultraviolet radiation from nearby stars or other cosmic radiation sources.

The number of laboratory studies on the photoionization of ions is limited because the production of ionic targets with sufficient densities for meaningful photoionization and photofragmentation experiments is challenging. Experiments with atomic ions which employed the photon-ion merged-beams technique have been reviewed repeatedly [5–7]. Experimental inner-shell studies with molecular ions are even more scarce. Previous work has been carried out on the photoionization and photofragmentation of cluster ions (e.g., [8]), endohedral fullerene ions [9], biomolecular ions (e.g., [10,11]), and polycyclic aromatic hydrocarbons [12].

Recently, inner-shell studies have been reported also on small molecular ions containing hydrogen, i.e., on the molecular cations CH^+, OH^+, and SiH^+ [13]. Here we investigate the photoabsorption of a similar diatomic ion, IH^+, via excitation or ionization of the iodine 3*d* shell. In x-ray studies on dynamic processes, iodine-containing molecules have attracted considerable interest since the massive iodine atom slows down the fragmentation process, bringing the time-dependent dynamics onto time scales accessible by free-electron laser sources [14]. Furthermore, iodine-containing molecules can be efficiently excited by soft x-rays via the strong iodine 3*d* and 4*d* resonances (e.g., [15,16]). Therefore, we have chosen the IH^+ ion as a model system to utilize the iodine 3*d*-electron excitation for probing the molecular valence orbitals.

Previous work involving photoexcitation of the iodine 3*d* shell has been carried out by Hashmall *et al.* [17], who examined the chemical shift in photoelectron emission from the 3*d* orbital in dependence of the type of ligand of the iodine atom. Hitchcock and Brion [18] measured the absorption cross section of CH_3I around the 3*d* ionization threshold using electron energy-loss spectroscopy. Aksela *et al.* [19] measured the Auger electron spectra resulting from 3*d* excitation of I and I_2. Most recently, photofragmentation and photoionization of neutral I_2 molecules was studied by Boo and Saito [20].

For the comparison with the I^{q+} ($q = 2 - 7$) ion yields resulting from photofragmentation of molecular IH^+ ions, we have also measured relative cross sections for multiple photoionization of atomic I^+ ions leading to the production of I^{q+} ions with $q = 2$–8. This greatly aids in disentangling atomic and molecular effects in the IH^+ spectra. For the further interpretation of the molecular spectra, we have performed corresponding theoretical calculations. The present paper is

*stephan.klumpp@desy.de
†michael.martins@desy.de

organized as follows. In Sec. II the experimental procedures are briefly described. The results are presented and discussed in Sec. III. A closing summary is given in Sec. IV.

II. EXPERIMENT

The present experiments on IH^+ and I^+ ions were carried out by employing the photon-ion merged-beams method (e.g., [7]) at the photon-ion spectrometer at PETRA III (PIPE). PIPE is a permanently installed end-station at beamline P04 [21] of the PETRA III synchrotron radiation facility at DESY in Hamburg, Germany. Detailed descriptions of the PIPE setup can be found in Refs. [22] and [23]. Here only specific procedures related to the present experiment are described.

The I^+ and IH^+ ions were produced from evaporated liquid CH_3I in a 10-GHz electron cyclotron-resonance ion source which was kept on a potential of 6000 V. Upon extraction, the ions were accelerated towards the ion beamline, which is on ground potential. A dipole magnet was used for selecting the desired mass-to-charge ratio for further transport to the photon-ion interaction region. The mass-resolving power of our mass spectrometer can be selected by adjusting entrance and exit slits. In the present experiment the mass-resolving power was $m/(\Delta m) \approx 710$. This was sufficient for separating IH^+ and I^+, as shown in Fig. 1.

In the photon-ion interaction region the ion beam was directed onto the photon beam such that the ions propagated on the photon-beam axis along a merging section of about 1.7 m length. The ions were excited with monochromatized synchrotron radiation with photon energies E ranging from 610 to 680 eV. This range comprises the iodine $3d_{5/2}$ and $3d_{3/2}$ ionization thresholds. For neutral iodine these thresholds are located at 619.3 and 630.8 eV, respectively [24]. In the P04 monochromator, a 400-lines/mm variable line spacing (VLS) grating was used to disperse the photons from the P04 undulator. The exit slit of the monochromator was set to a width of 1500 μm, resulting in a resolving power $E/(\Delta E) \approx 600$. The

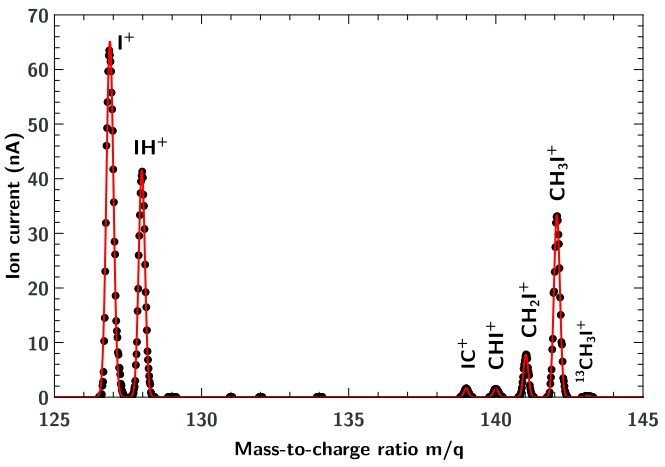

FIG. 1. Mass spectrum of ions produced from CH_3I obtained by scanning the magnetic field of the dipole magnet. The singly charged atomic iodine ion $^{127}I^+$ is clearly separated from the $^{127}I^1H^+$ molecular ion. The solid (red) line results from a fit of seven Gaussian functions to the experimental data. From the fit the mass-resolving power was determined to be $m/(\Delta m) \approx 710$ in this measurement.

absolute energy scale of the monochromator was calibrated using Ne $1s \rightarrow 3p/4p$ and Xe $3d_{5/2} \rightarrow 6p$ transitions and taking the Doppler shift due to the ion motion into account. The resulting uncertainty of the experimental photon-energy scale is estimated to be approximately 1 eV.

Ionic fragments I^{q+} ($q \geqslant 2$) emerging from the photon-ion interaction region were charge separated by a second dipole magnet, and I^{q+} product ions with the selected charge state q were counted with a channeltron-based single-particle detector. The light H^+ fragments could not be directed efficiently into the detector because they received too much transverse momentum upon molecular breakup, as will be discussed below. Neutral fragments were not detected either, since these cannot be deflected by the second magnet and, thus, continue to propagate on the photon-beam axis.

III. RESULTS AND DISCUSSION

Figure 2 shows ion-yield curves for the parent ions I^+ [red, panel (a)] and IH^+ [blue, panel (b)] summed over all measured fragment channels producing I^{q+} ions ($q = 2$–8 for I^+ and $q = 2$–7 for IH^+). Here, only these sum spectra are

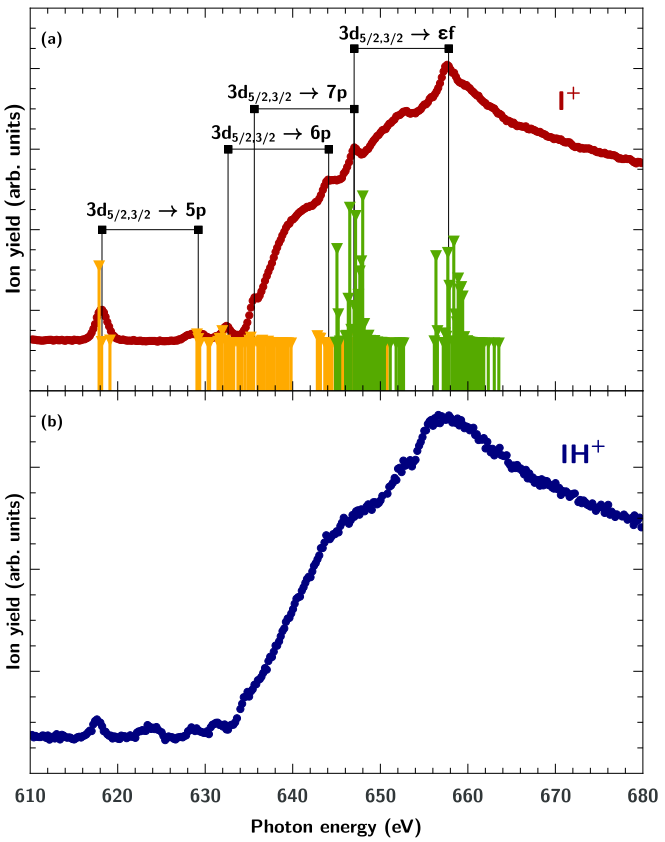

FIG. 2. Ion-yield curves for the primary target ions I^+ (red, panel a) and IH^+ (blue, panel b) summed over all measured fragment channels I^{q+} ($q = 2$–8 for I^+ and $q = 2$–7 for IH^+). According to a Hartree-Fock (HF) calculation [31] for I^+ (vertical solid lines), the narrow resonances can be assigned to the $3d_j - np$ ($j = 3/2, 5/2$; $n = 5, 6, 7$) excitations and the two broad resonance features are due to the $3d_j \rightarrow \varepsilon f$ shape resonances. The energy axis of the HF calculation was shifted to match the energetically lowest resonance of the experimental I^+ ion-yield curve.

discussed. The IH^+ curve is normalized to the I^+ yield at 680 eV. The overall shape of both curves resembles the $3d$ absorption spectra of Xe [25], Xe^+ [22], I_2 [20], and CH_3I [18]. Small narrow resonance features are found at energies below approximately 635 eV. Above this energy the onset of a strong quasicontinuum of absorption is observed, which is mainly due to the direct photoionization of the $3d$ subshell and the two well-known $3d_j \rightarrow \varepsilon f$ shape resonances producing either a $3d_{3/2}$ or a $3d_{5/2}$ vacancy. The spin-orbit splitting of the $3d_j$ hole states is ∼11 eV, and because of their large widths of the order of 10 eV, the $3d$ ionization edge is smeared out.

The atomic iodine curve features several narrow resonance peaks above the $3d$ ionization threshold, while the IH^+ curve is relatively smooth in this energy range. When normalized to the ion current of the primary ion beam, the count rate for the photoabsorption of the IH^+ is lower compared to the I^+ count rate by a factor of about 3. This is due to a reduced transmission of the I^{q+} ($q \geqslant 2$) products caused by the kinetic energy release (KER) upon fragmentation of the IH^+ molecular ions. Assuming one localized charge each on the iodine and the hydrogen after photoionization and assuming an IH^+ bond length of 1.65 Å [26,27], the repulsive energy due to the Coulomb interaction is 8.6 eV. Due to the associated KER, the charged fragments acquire an additional momentum which, in the worst case, can be in transversal direction. Hence, a considerable fraction of the fragment ions is cut off by the narrow acceptance of the second dipole magnet. According to a more quantitative geometric estimation, the H^+ fragments will be almost completely lost at the entrance aperture and only a part of the iodine fragments I^{q+} can pass it and reach the detector. This is a common issue in experiments employing molecular-ion beams [13,28], which, in principle, can be overcome by choosing a detection system with a sufficiently large angular acceptance [29,30].

To identify the resonances observed in the absorption spectrum of the atomic target ion I^+, Hartree-Fock (HF) calculations [31] have been performed (vertical lines in Fig. 2). These calculations suggest that the narrow features in the spectrum can be assigned to the core-to-valence excitation $3d_j \rightarrow 5p$ and the Rydberg resonances $3d_j \rightarrow np$ ($j = 5/2$, $3/2$; $n = 6$, 7) with a $3d$ spin-orbit splitting (indicated with vertical lines also in Fig. 2) of 10.8 ± 0.3 eV. This value agrees within the error bars with the 11.5 ± 0.6 eV reported for neutral iodine [24].

In Fig. 3, the calculated I^+ spectra in the pre-edge region are depicted for the atomic $I^+(5p^4\ ^3P_{2,1,0})$ initial levels which are populated in the I^+ beam with their statistical weights. The excitation from these three initial levels results in a broadening of the $3d_{5/2} \rightarrow 5p$ resonance A. For the $3d_{3/2} \rightarrow 5p$ resonance B, the spin-orbit splitting of the initial ^3P term causes the observed asymmetry. Rydberg levels with $n > 7$ could not be identified experimentally, because the higher n members of the Rydberg series are superimposed by the $3d$ ionization threshold and the $3d \rightarrow \varepsilon f$ resonances.

A first assignment of the resonances observed in the IH^+ molecular ion can be made by comparison with the spectrum of the atomic I^+ ion. The ground state of the IH molecule has been assigned [32,33] to the term

$$KLMN\,(5s\sigma)^2\,(5p\sigma)^2\,(5p\pi)^4\,{}^1\Sigma_g^+,$$

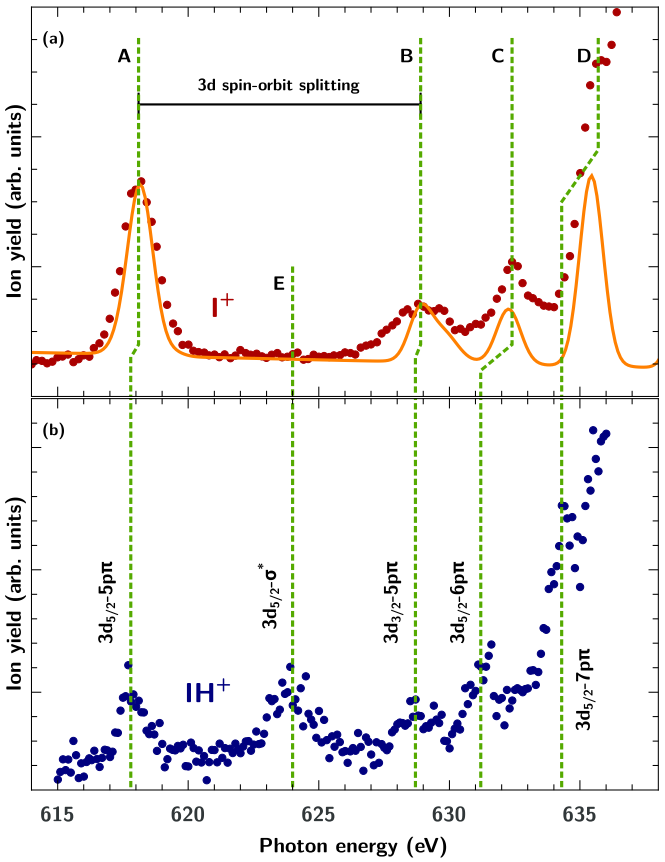

FIG. 3. Comparison of the summed ion yields for the parent ions I^+, shown as lighter shaded (red) dots (panel a), and for IH^+, shown as dark shaded (blue) dots (panel b), resulting from photoexcitation in the energy range below the iodine $3d$ ionization threshold. In the ion-yield spectrum of the molecular ion an additional resonance appears (peak E). The molecular resonances are all shifted in energy, as indicated by the vertical dark (green) dotted lines. The values for these chemical shifts are given in Table I. The full (orange) line (in panel a) is the calculated photoabsorption for I^+ originating from the weighted sum of the different I^+ initial states $5p^4\ ^3P_J$, with $J = 0,1,2$ obtained by Hartree-Fock calculations.

from which the following levels [34] can be derived for the IH^+ molecule with a $(5p\,\pi)$ electron removed:

$$KLMN\,(5s\sigma)^2\,(5p\sigma)^2\,(5p\pi)^3\,{}^2\Pi_{3/2,1/2}.$$

The $^2\Pi_{3/2}$ level is the ionic ground level. Hence, the first peak marked A in Fig. 3 can be assigned to a transition from

TABLE I. Peak assignments and chemical shifts for the atomic iodine resonances A–D in Figs. 2 and 3. The quoted uncertainties resulted from numerical fits of Gaussian functions to the experimental peaks (see text).

Peak label	Assignment	Chemical shift (eV)
A	$3d_{5/2} - (5p\,\pi)$	0.3 ± 0.2
B	$3d_{3/2} - (5p\,\pi)$	0.2 ± 0.3
C	$3d_{5/2} - (6p\,\pi)$	1.2 ± 0.2
D	$3d_{5/2} - (7p\,\pi)$	1.1 ± 0.4

the inner-shell atomic iodine $3d_{5/2}$ orbital into the molecular $(5p\,\pi)$ valence orbital, which is analogous to the $5p$ resonance in I^+. Peak B is the corresponding spin-orbit split line. The next accessible molecular orbital of IH above the $(5p\,\pi)$ orbital is a σ^* orbital [35], which we observe as a feature at 624 eV in the ion-yield curve of IH^+ (peak E in Fig. 3). Peak E is not present in the absorption spectrum of atomic I^+. The valence σ^* orbital arises from the hybridization of the iodine and hydrogen valence orbitals. In analogy to the designations for the atomic I^+ ion we assign peaks C and D tentatively to molecular np Rydberg levels.

Due to the influence of the bound hydrogen atom, the molecular resonances are shifted in energy relative to the I^+ resonances as indicated by the vertical dotted lines in Fig. 3. The chemical shift for the $3d_{5/2} - (5p\,\pi)$ resonance in the IH^+ molecular ion relative to the $3d_{5/2} - 5p$ resonance in I^+ is 0.3 ± 0.2 eV (peak labeled A in Fig. 3). For peak B the chemical shift is 0.2 ± 0.3 eV which is, within the uncertainty of the fit, identical with the shift of peak A and agrees with the assumption that B is the spin-orbit split counterpart of A, namely, the $3d_{3/2} - (5p\,\pi)$ resonance. Peak C can be assigned to the transition from $3d_{5/2}$ to $(6p\,\pi)$ and has a chemical shift of 1.2 ± 0.2 eV. Peak D is assigned to $3d_{5/2} - (7p\,\pi)$ and has a chemical shift of 1.1 ± 0.4 eV. For extracting the chemical shifts, all lines have been fitted by Gaussians (accounting for the broad bandwidth of the excitation photons) on top of a sigmoidal "background", accounting for the cross-section rise at the $3d$ ionization threshold.

For the molecular IH^+ ion it can be assumed that the halogen iodine has a higher electronegativity than the hydrogen. The additional electron from the hydrogen in the valence orbital of IH^+ will hence have a higher probability to reside at the iodine site than at the hydrogen site. Effectively, the electron from hydrogen in IH^+ will partially screen the core charge of iodine compared to the pure I^+ cation. Hence, all molecular orbitals with a strong iodine atomic characteristic, including the core $3d$ levels, will shift to lower binding energies. Thus, the corresponding transition energies from the core to the unoccupied levels will decrease since the energy shift of the core levels is larger.

To verify this tentative assignment of the $3d$ excited levels of IH^+ in the energy region below the $3d$ ionization threshold, the electronic structure and the iodine $3d$ excitation spectra were calculated within density functional theory (DFT) as implemented in the ADF-2017 program package [36,37]. The largest available quadruple-zeta with four polarization functions (QZ4P) basis set [38] was additionally extended by five polarization functions for the proper description of the iodine $6p$ and $7p$ states. Several exchange correlation functionals were tested, including pure Hartree-Fock, local GGA-PBE [39], hybrid B3LYP [40] and KMLYP [41] with 20% and 55.7% of exact exchange, respectively, and meta-GGA M06HF [42] with 100% HF exchange. Among the DFT simulations, KMLYP showed the best agreement to the experimental spectrum of atomic I^+ but still exhibits less agreement compared to the multiplet HF calculation [compare Figs. 3(a) and 5(a)]. The results using the KMLYP functional were then used for the subsequent assignment of the IH^+ transitions. The interatomic distance of 1.62 Å obtained with KMLYP and the 12.1-eV spin-orbit splitting of the iodine $3d$ states are in good

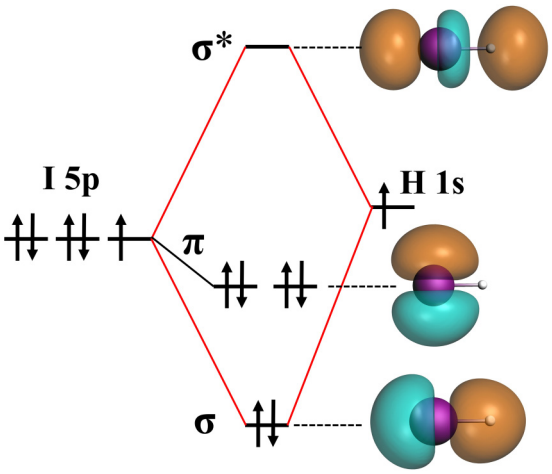

FIG. 4. Molecular orbital diagram for neutral IH as obtained by the DFT simulation.

agreement with literature data [24]. Electron transition energies and oscillator strengths were calculated within the Tamm-Dancoff approximation for the time-dependent DFT [43,44], including spin-orbit effects. The absolute energy values of the calculated spectra were shifted by 0.6 eV using peak A in the experimental spectra as reference and convoluted with a 1.0 eV (FWHM) Gaussian.

Figure 4 shows the molecular orbital diagram for the neutral IH molecule. Iodine is a halogen atom so it attracts the electron from the hydrogen when the chemical bond is formed, filling its $5p$ shell completely. However, as shown in Fig. 4 for the σ molecular orbital, the effective size of the $5p$ orbital matches the I-H bond length. The real charge transfer from H to I is thus small. This fact is confirmed by the $3d_{5/2}$ core-level energy shift shown in Table II. For IH the energy-level shift is only 0.2 eV relative to I, while for the charged I^+ and IH^+ it is -9.6 eV and -9.0 eV, respectively. Hence, the shift of IH^+ relative to I^+ is 0.6 eV. The larger chemical shift in the ionized species can be explained by the contracted size of the $5p$ orbitals, which increase the charge transfer from the hydrogen to the iodine upon filling the iodine $5p$ shell.

Figure 5 shows the comparison of the experimental data (dots) with the calculated x-ray absorption spectra (solid lines) and Fig. 6 the molecular orbital isosurfaces responsible for the transitions.

From the DFT calculations the peaks A and B can be assigned to the $3d_{5/2} \rightarrow (5p\,\pi)$ and $3d_{3/2} \rightarrow (5p\,\pi)$ transitions involving the iodine $5p_x$ and $5p_y$ orbitals. The iodine $5p_z$ orbital is hybridized with the hydrogen $1s$ orbital and forms an antibonding σ^* orbital responsible for transitions E in the absorption spectrum (see Figs. 4 and 6). Peak C can be attributed to the transition $3d_{5/2} \rightarrow (6p\,\pi)$ hybridized of

TABLE II. Calculated energy shift of the $3d_{5/2}$ levels in eV for the neutral IH molecule and the I^+ and IH^+ cations relative to the neutral iodine atom I.

I	IH	I^+	IH^+
0	0.2 eV	-9.6 eV	-9.0 eV

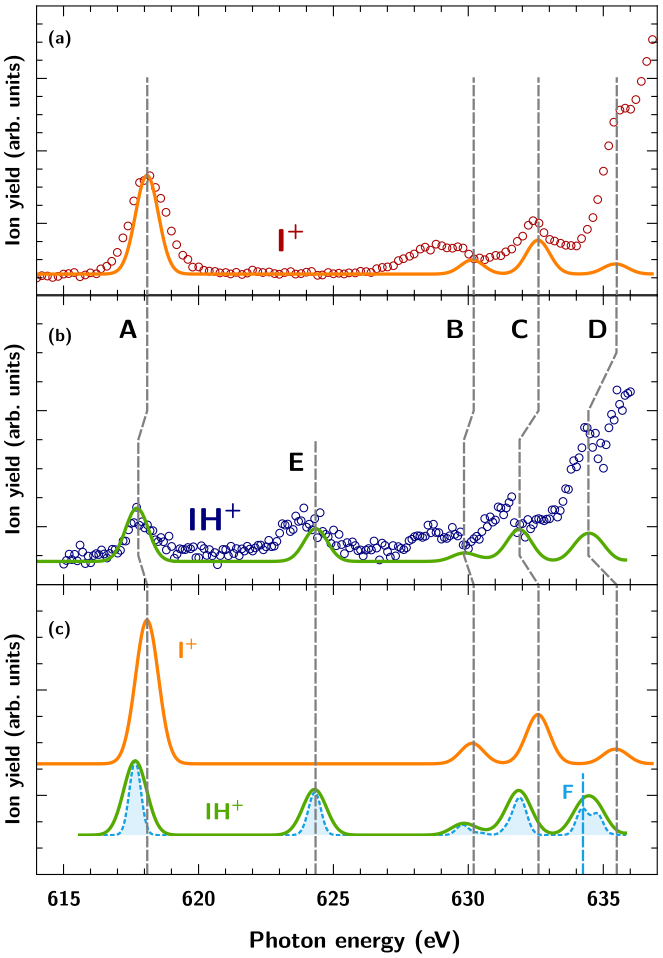

FIG. 5. Results of the DFT simulation with the KMLYP functional (see text). (a) I^+: Measured ion yield (red open dots) and calculated spectrum (solid orange line). (b) IH^+: Measured ion yield (blue open dots) and calculated spectrum (solid green line). (c) Comparison of the calculated spectra for I^+ (orange solid line) and IH^+ (solid green line) from (a) and (b). The gray dashed vertical lines mark the peaks calculated by DFT of the I^+ and IH^+ spectrum. The light blue, dashed line is the simulated IH^+ spectrum but convoluted with a 0.5 eV Gaussian function. An additional line (peak F) becomes visible which is not resolved in the experiment. Line assignment according to the DFT calculations for IH^+: (A) $3d_{5/2} \rightarrow (5p\,\pi)$, (B) $3d_{3/2} \rightarrow (5p\,\pi)$, (C) $3d_{5/2} \rightarrow (6p\,\pi)$, (D) $3d_{5/2} \rightarrow (7p\,\pi)$, (E) $3d_{5/2} \rightarrow \sigma^*$, and (F) $3d_{5/2} \rightarrow \sigma^*$.

the iodine $(6p_x + 5d_{xz})$, $(6p_y + 5d_{yz})$, and of the hydrogen $2p_x$ and $2p_y$ orbitals, while peak D can be attributed to $3d_{5/2} \rightarrow (7p\,\pi)$ weakly hybridized by the interaction of the iodine $7p_x$ and $7p_y$ and the hydrogen $2p_x$ and $2p_y$ orbitals. Peak F, consisting of iodine $5p_z$ and $5d_{z^2}$ and hydrogen $2s$ and $2p_z$ orbitals, is predicted theoretically but is not resolved in the experimental data. It is attributed to an antibonding σ^* molecular orbital.

A chemical shift is observed between the theoretical spectra for I^+ and IH^+ [Fig. 5(c)]. Peaks A–D observed in IH^+ originate from similar atomic orbitals and are shifted to lower energies as compared to I^+. The calculated value of this shift is larger for peaks C and D (0.7 eV) than for A and B (0.4 eV). Qualitatively this can be understood in terms of

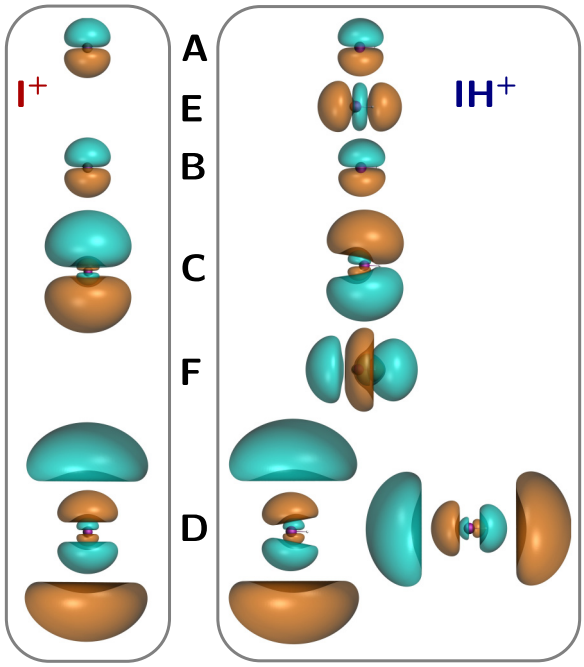

FIG. 6. Calculated isosurfaces for the atomic and molecular orbitals. The assignment of the final states of the observed transitions labeled A–E can be found in the caption of Fig. 5. (F) The σ^* molecular orbital is not resolved in the experiment. The isosurface values are identical for all orbitals, the two colors indicating the positive or negative sign of the wave function.

the different size of molecular orbitals responsible for the transitions A, B and C, D. The core charge of the iodine in IH^+ is partially screened by means of the σ orbital, shown in Fig. 4. Due to its smaller size, the molecular orbital A and its spin-orbit counterpart B experience a larger energy shift than the delocalized C and D orbitals. Thus, the resulting difference between the energy of the core $3d_{5/2}$ orbital (which is also subjected to chemical shift) and the corresponding unoccupied molecular orbitals will be smaller for A, B than for C and D. The excitations shown in the theoretical spectrum include transitions to the hybridized iodine p and d and hydrogen s and p states. Higher excitations would require iodine f orbitals to be considered. Such calculations are beyond the scope of the present article and DFT should be used with special care there. The first issue here is the limited quality of the time-dependent functionals presently available for the excited-state calculations, in contrast to the rapid development of a large variety of reliable ground-state functionals. The second issue is related to the many-body effects on $d-f$ transitions, including the $4f$ wave-function collapse (e.g., [45]) where multiconfigurational approaches should be used.

IV. SUMMARY

Ion yields after photoexcitation and photoionization of the singly charged atomic I^+ and molecular IH^+ ions have been measured by recording the I^{q+} $(q \geqslant 2)$ product-ion yields and adding them together. In the energy region below the iodine $3d$ ionization threshold, resonances have been observed which can be attributed to $3d \rightarrow np\,(n = 5, 6, 7)$ transitions for the atomic

parent ion. The iodine I^+ $3d^{-1}np$ levels show a spin-orbit splitting of the order of 10.8 ± 0.3 eV. For the molecular cation IH^+, in addition to the resonances observed with atomic iodine ions, one more resonance is found which is caused by the hybridization of the iodine and hydrogen orbitals. Using DFT calculations we assigned this resonance to a transition of a $3d_{5/2}$ inner-shell electron to an antibonding σ^* orbital. The $(np\,\pi)$ resonances observed in the IH^+ spectrum show a chemical shift compared to corresponding resonances in the atomic ion I^+, caused by the hydrogen atom bonded to the iodine, of the order of 0.3 eV (averaged) for the almost atomlike $(5p\,\pi)$ levels, whereas for the $(6p/7p\,\pi)$ molecular Rydberg levels a 3–4 times larger shift is observed. Simulations using DFT can predict the relative chemical shift to lower binding energies from the I^+ to the IH^+ ion as observed in the experiment. The increased energy shift for the $6p/7p$ excitations compared to $5p$ can be understood in terms of the larger size of the molecular orbitals responsible for these transitions. Both $3d$ core levels and unoccupied orbitals experience a chemical shift when the hydrogen atom bonds to the I^+. Due to its smaller size, the molecular orbital A and its spin-orbit counterpart B experience a larger energy shift than the delocalized C and D orbitals. Thus, the resulting difference between the energy of the $3d_{5/2}$ core orbital and the corresponding unoccupied molecular orbitals will be smaller for A, B than for C and D.

To conclude, we were able to show that the resonances in the iodine $3d$ pre-edge regime are sensitive to the molecular electronic state, as can be seen from the different values for the chemical shift of the lines observed. Due to this sensitivity these lines might be exploited in various iodine-containing molecules to examine the dynamics of electron excitation using inner-shell x-ray spectroscopy. Furthermore, we have demonstrated that the photon-ion merged-beams method as implemented at the PIPE setup can be employed for the inner-shell absorption spectroscopy of mass-selected molecular ions. The accuracy of the present measurements on IH^+ ions was mainly limited by the counting statistics. We are confident that further improvements of our experimental apparatus and, in particular, of our ion-source technology will, in the future, facilitate even more precise spectroscopic studies of molecular ions at the PIPE setup.

ACKNOWLEDGMENTS

This research was carried out at the synchrotron light source PETRA III at DESY, a member of the Helmholtz Association (HGF). We would like to thank L. Glaser, G. Hartmann, F. Scholz, J. Seltmann, and J. Viefhaus for assistance in using beamline P04. The PIPE setup and this work have been funded by the Bundesministerium für Bildung und Forschung (BMBF) under Contracts No. 05KS7RG1, No. 05KS7GU2, No. 05KS7KE1, No. 05KS7RF2, No. 05K10RG1, No. 05K10GUB, No. 05K10KEA, No. 05K10RF2, No. 05K13GUA, and No. 05K13GUB within the Verbundforschung funding scheme. Further funding by the Deutsche Forschungsgemeinschaft (DFG) via SFB925/A3 is acknowledged. S.K. acknowledges support from the European Cluster of Advanced Laser Light Sources (EUCALL) project, which has received funding from the European Union's Horizon 2020 Research and Innovation program under Grant Agreement No. 654220. S.B. and K.S. are thankful for funding from the Initiative and Networking Fund of the Helmholtz Association and acknowledge financial support by the DFG through Sonderforschungsbereich SFB755 Nanoscale Photonic Imaging. A.A.G. acknowledges a grant from the Southern Federal University (VnGr-07/2017-08) for financial support.

[1] D. Aurbach, Y. Talyosef, B. Markovsky, E. Markevich, E. Zinigrad, L. Asraf, J. S. Gnanaraj, and H.-J. Kim, Electrochim. Acta **50**, 247 (2004).
[2] R. K. O. Sigel and A. M. Pyle, Chem. Rev. **107**, 97 (2007).
[3] M.-F. Lin, A. N. Pfeiffer, D. M. Neumark, S. R. Leone, and O. Gessner, J. Chem. Phys. **137**, 244305 (2012).
[4] M. Larsson, W. D. Geppert, and G. Nyman, Rep. Prog. Phys. **75**, 066901 (2012).
[5] H. Kjeldsen, J. Phys. B **39**, R325 (2006).
[6] A. Müller, Phys. Scr. **90**, 054004 (2015).
[7] S. Schippers, A. L. D. Kilcoyne, R. A. Phaneuf, and A. Müller, Contemp. Phys. **57**, 215 (2016).
[8] J. T. Lau, J. Rittmann, V. Zamudio-Bayer, M. Vogel, K. Hirsch, P. Klar, F. Lofink, T. Möller, and B. von Issendorff, Phys. Rev. Lett. **101**, 153401 (2008).
[9] J. Hellhund, A. Borovik, Jr., K. Holste, S. Klumpp, M. Martins, S. Ricz, S. Schippers, and A. Müller, Phys. Rev. A **92**, 013413 (2015).
[10] O. González-Magaña, M. Tiemens, G. Reitsma, L. Boschman, M. Door, S. Bari, P. O. Lahaie, J. R. Wagner, M. A. Huels, R. Hoekstra, and T. Schlathölter, Phys. Rev. A **87**, 032702 (2013).
[11] A. R. Milosavljević, F. Canon, C. Nicolas, C. Miron, L. Nahon, and A. Giuliani, J. Phys. Chem. Lett. **3**, 1191 (2012).
[12] G. Reitsma, L. Boschman, M. J. Deuzeman, O. González-Magaña, S. Hoekstra, S. Cazaux, R. Hoekstra, and T. Schlathölter, Phys. Rev. Lett. **113**, 053002 (2014).
[13] J.-P. Mosnier, E. T. Kennedy, P. van Kampen, D. Cubaynes, S. Guilbaud, N. Sisourat, A. Puglisi, S. Carniato, and J.-M. Bizau, Phys. Rev. A **93**, 061401 (2016).
[14] S. Minemoto, T. Teramoto, H. Akagi, T. Fujikawa, T. Majima, K. Nakajima, K. Niki, S. Owada, H. Sakai, T. Togashi, K. Tono, S. Tsuru, K. Wada, M. Yabashi, S. Yoshida, and A. Yagishita, Sci. Rep. **6**, 38654 (2016).
[15] B. Erk, R. Boll, S. Trippel, D. Anielski, L. Foucar, B. Rudek, S. W. Epp, R. Coffee, S. Carron, S. Schorb, K. R. Ferguson, M. Swiggers, J. D. Bozek, M. Simon, T. Marchenko, J. Küpper, I. Schlichting, J. Ullrich, C. Bostedt, D. Rolles, and A. Rudenko, Science **345**, 288 (2014).
[16] K. Mertens, N. Gerken, S. Klumpp, M. Braune, and M. Martins, J. Mod. Opt. **63**, 383 (2016).
[17] J. A. Hashmall, B. E. Mills, D. A. Shirley, and A. Streitwieser, J. Am. Chem. Soc. **94**, 4445 (1972).
[18] A. Hitchcock and C. Brion, J. Electron Spectrosc. Relat. Phenom. **13**, 193 (1978).
[19] S. Aksela, H. Aksela, and T. D. Thomas, Phys. Rev. A **19**, 721 (1979).

[20] B. H. Boo and N. Saito, J. Electron Spectrosc. Relat. Phenom. **127**, 139 (2002).
[21] J. Viefhaus, F. Scholz, S. Deinert, L. Glaser, M. Ilchen, J. Seltmann, P. Walter, and F. Siewert, Nucl. Instrum. Methods A **710**, 151 (2013).
[22] S. Schippers, S. Ricz, T. Buhr, A. Borovik, Jr., J. Hellhund, K. Holste, K. Huber, H.-J. Schäfer, D. Schury, S. Klumpp, K. Mertens, M. Martins, R. Flesch, G. Ulrich, E. Rühl, T. Jahnke, J. Lower, D. Metz, L. P. H. Schmidt, M. Schöffler *et al.*, J. Phys. B **47**, 115602 (2014).
[23] A. Müller, D. Bernhardt, A. Borovik, Jr., T. Buhr, J. Hellhund, K. Holste, A. L. D. Kilcoyne, S. Klumpp, M. Martins, S. Ricz, J. Seltmann, J. Viefhaus, and S. Schippers, Astrophys. J. **836**, 166 (2017).
[24] J. A. Bearden and A. F. Burr, Rev. Mod. Phys. **39**, 125 (1967).
[25] R. D. Deslattes, Phys. Rev. Lett. **20**, 483 (1968).
[26] L. Zhu, V. Kleiman, X. Li, S. P. Lu, K. Trentelman, and R. J. Gordon, Science **270**, 77 (1995).
[27] A. J. Cormack, A. J. Yencha, R. J. Donovan, K. P. Lawley, A. Hopkirk, and G. C. King, Chem. Phys. **221**, 175 (1997).
[28] G. Hinojosa, M. M. Sant'Anna, A. M. Covington, R. A. Phaneuf, I. R. Covington, I. Domínguez, A. S. Schlachter, I. Alvarez, and C. Cisneros, J. Phys. B **38**, 2701 (2005).
[29] Z. Amitay, D. Zajfman, P. Forck, U. Hechtfischer, B. Seidel, M. Grieser, D. Habs, R. Repnow, D. Schwalm, and A. Wolf, Phys. Rev. A **54**, 4032 (1996).
[30] L. Lammich, C. Domesle, B. Jordon-Thaden, M. Förstel, T. Arion, T. Lischke, O. Heber, S. Klumpp, M. Martins, N. Guerassimova, R. Treusch, J. Ullrich, U. Hergenhahn, H. B. Pedersen, and A. Wolf, Phys. Rev. Lett. **105**, 253003 (2010).
[31] R. D. Cowan, *The Theory of Atomic Structure and Spectra* (California University Press, Berkeley, CA, 1981).
[32] R. S. Mulliken, Phys. Rev. **46**, 549 (1934).
[33] D. C. Frost and C. A. McDowell, Can. J. Chem. **36**, 39 (1958).
[34] P. Baltzer, L. Karlsson, S. Svensson, and B. Wannberg, J. Phys. B **23**, 1537 (1990).
[35] D. S. Ginter, M. L. Ginter, and S. G. Tilford, J. Mol. Spectrosc. **92**, 40 (1982).
[36] G. te Velde, F. M. Bickelhaupt, E. J. Baerends, C. Fonseca Guerra, S. J. A. van Gisbergen, J. G. Snijders, and T. Ziegler, J. Comput. Chem. **22**, 931 (2001).
[37] C. F. Guerra, J. G. Snijders, G. te Velde, and E. J. Baerends, Theor. Chem. Acc. **99**, 391 (1998).
[38] E. Van Lenthe and E. J. Baerends, J. Comput. Chem. **24**, 1142 (2003).
[39] J. P. Perdew, K. Burke, and M. Ernzerhof, Phys. Rev. Lett. **77**, 3865 (1996).
[40] M. Reiher, O. Salomon, and B. A. Hess, Theor. Chem. Acc. **107**, 48 (2001).
[41] J. K. Kang and C. B. Musgrave, J. Chem. Phys. **115**, 11040 (2001).
[42] Y. Zhao and D. G. Truhlar, J. Phys. Chem. A **110**, 13126 (2006).
[43] S. van Gisbergen, J. Snijders, and E. Baerends, Comput. Phys. Commun. **118**, 119 (1999).
[44] S. Hirata and M. Head-Gordon, Chem. Phys. Lett. **314**, 291 (1999).
[45] S. Schippers, A. Borovik, Jr., T. Buhr, J. Hellhund, K. Holste, A. L. D. Kilcoyne, S. Klumpp, M. Martins, A. Müller, S. Ricz, and S. Fritzsche, J. Phys. B **48**, 144003 (2015).